

Surface Properties and Structural Collapse of Silica in Matte Water-Based Lacquers

C. Patrick Royall and Athene M. Donald*

Cavendish Laboratory, The University of Cambridge, Madingley Road, Cambridge, CB3 0HE, United Kingdom

Received March 26, 2002. In Final Form: August 28, 2002

An investigation into the relationship between surface microstructure and optical properties of matte water-based lacquer is presented, and a model describing this relationship in terms of the packing of silica matting agent is tested. This model assumes that, at some critical concentration, the silica structure in the film-formed lacquer is similar to that found in the dry powder. Above this critical concentration, an increase in surface roughness is expected, which is related to the reflectance of the lacquer. The lacquer surface is accessed via environmental scanning electron microscopy and atomic force microscopy, and the results are related to the model described and the reflectance measured. The reflectance is found to be inversely related to the surface roughness. The prediction for increase in surface roughness above the critical silica concentration is shown to be valid for robust precipitated silicas with large (10 μm) aggregate particles. Smaller 2 μm aggregate particles show a much reduced surface roughness. A difference in behavior is seen between fumed and precipitated silicas. Fumed silica undergoes total structural collapse at high silica concentration, with a limited quantity of silica around the surface. With precipitated silica, the collapse is much less complete, and more silica is present near the surface at high silica concentrations.

1. Introduction

Polymer latices, the basis of many water-based lacquers, have been studied for half a century. Although the film formation process from a latex suspension to a continuous polymer film is not fully understood, a number of mechanisms have been identified. For film formation to proceed, the aqueous latex suspension is laid down on a substrate, and water is removed through evaporation, leaving a densely packed array of latex spheres. These deform to produce a continuous polymer layer. Typically this deformation occurs at the same time as the water evaporation. On a longer time scale, polymer chains interdiffuse between the latex particles.¹

This article is specifically concerned with matte water-based lacquers and examines one of their defining properties, surface roughness.² For the lacquers under consideration here, the surface roughness is introduced by incorporating silica into the latex in the form of particles in the 1–10 μm size range. This silica causes surface roughness on the length scale of visible light, causing a loss of reflection, or matting.

A model has been developed³ to describe the structure taken up by the silica and is extended to consider different types of silica. Essentially this model assumes that, at a certain critical concentration of silica in the lacquer, the process of lacquer formulation and subsequent film formation leads to the situation that all the air between the silica particles in the initial dry powder is replaced with polymer in the final film-formed lacquer. A volume-based argument allows the derivation of this critical silica concentration, which is expressed as a mass fraction of the lacquer formulation. At this critical silica concentration, there should be a silica structure similar to that found

in the dry powder. The silica structure formed in the bulk of the film has been verified directly via confocal microscopy.⁴

This article considers the surface structure, accessed via atomic force microscopy (AFM)⁵ and environmental scanning electron microscopy (ESEM).⁶ While AFM provides a nanometer-resolution surface map of a small region, ESEM can image a wider, more typical area of the specimen. Unlike conventional SEM, ESEM allows the imaging of insulating samples without potentially damaging sample preparation.

Having determined the microstructure, the model is tested through computational image analysis techniques. The numerical data extracted can be related to the optical properties, in particular specular reflection, which distinguishes matte lacquers. In fact, reflection has been related to surface roughness by Gate et al.⁷ These workers found evidence supporting a relationship between the standard deviation of height about the mean plane of a surface and the intensity of the reflected light given by

$$\ln \left(\frac{I_r}{I_0} \right) = -16\pi^2 \sigma^2 \frac{\cos^2 \theta}{\lambda^2} \quad (1)$$

where I_r and I_0 are reflected and incident light intensities, λ is the wavelength of the light, σ is the standard deviation of the surface, and θ is the angle to the normal of the incident beam. In this paper the standard deviation of the surface is extracted from AFM surface maps and together with reflection measurements compared with eq 1.

Two forms of synthetic amorphous silica are considered: fumed silica (FS) and precipitated silica (PS). Both silicas are formed of ultimate particles around 20 nm in

* To whom correspondence should be addressed: e-mail Amd3@phy.cam.ac.uk.

(1) Keddie, J. L. *Mater. Sci. Eng. R* **1997**, *21*, 101–170.

(2) Schneider, H. *Surf. Coatings Int.* **1994**, *77*, 376–385.

(3) Royall, C. P.; Donald, A. M. In *Film formation in coatings*; Provdor, T., Urban, M. W., Eds.; ACS Symposium Series; American Chemical Society: Washington, DC, 2001; Vol. 790, pp 193–211.

(4) Royall, C. P. *The behaviour of silica in matt water based lacquer*, Ph.D. Thesis, University of Cambridge, U.K., 2000.

(5) Sarid, D. *Scanning force microscopy, with applications to electric, magnetic and atomic forces*; Oxford Series in Optical and Imaging Sciences; Oxford University Press: Oxford, U.K., 1991.

(6) Danilatos, G. *Microsc. Res. Tech.* **1993**, *25*, 354–361.

(7) Gate L.; Windle, W.; Hine, M. *Tappi*, **1973**, *56* (3), 61–65.

diameter. The silicas are differentiated by the way in which they are aggregated into larger 1–10 μm particles. FS ultimate particles are only weakly bound through hydrogen bonding, resulting in a very voluminous low-density powder.^{8,9} PS, by contrast, has covalently bound ultimate particles resulting in rather denser, more robust aggregate particles. The precipitated silica is sieved into coarse and fine fractions (CPS and FPS, respectively). At the length scales considered here, it is the aggregate, rather than the ultimate, particles that are of interest.

2. Theory

As indicated above, the theory is centered around the volume occupied by the lacquer following film formation, during which water is lost through evaporation. At the level of this work, we neglect the interactions between the latex and silica particles. These will be reasonably small due to the somewhat acidic nature of the silica surface, which interacts relatively weakly with the slightly acidic latex.^{10,11} Equating the volume of polymer in the dry film with the volume of air accessible to the polymer latex particles in the dry silica powder should yield the critical concentration of silica as described above. At this silica concentration, when the air is exactly displaced by polymer, the silica structure is expected to be similar to that found in the dry powder, as shown in Figure 1b. The particles touch as in the dry powder and the structure percolates.

Well below the critical silica concentration, isolated particles are suspended in the polymer matrix, as shown in Figure 1a. These isolated silica particles do not percolate. Somewhere between the regimes in panels a and b of Figure 1, a percolation threshold is expected. Note that for the structure expected at the critical concentration, percolation is necessary, as in the dry powder this structure must support its own weight, but not sufficient, as a percolating structure may not support itself.

At higher concentrations, above the critical mass, silica collapse is expected for a weakly bound structure such as the fumed silica (Figure 1c). The alternative situation occurs for a robust silica structure, which resists volume reduction during film formation (Figure 1d) and which may also contain air voids in this case. In fact this noncollapsing possibility corresponds to the critical pigment volume concentration model of Asbeck and van Loo.¹² These workers described a similar approach for pigmented lacquers, effectively substituting pigment for silica. The approach here differs because the possibility of a collapsing structure is also considered and the bulk silica volume is determined accordingly from the dry powder. Asbeck and van Loo¹² extracted pigment from the dried lacquer to determine its volume.

Clearly, whether the silica structure collapses has significant implications for the surface roughness and therefore the optical properties of the lacquer. A collapsing structure (such as Figure 1c) need hardly disrupt the surface at all. By comparison, a totally robust structure (Figure 1d) may cause a very strong increase in surface roughness around the critical mass. This surface behavior may be probed with ESEM and AFM.

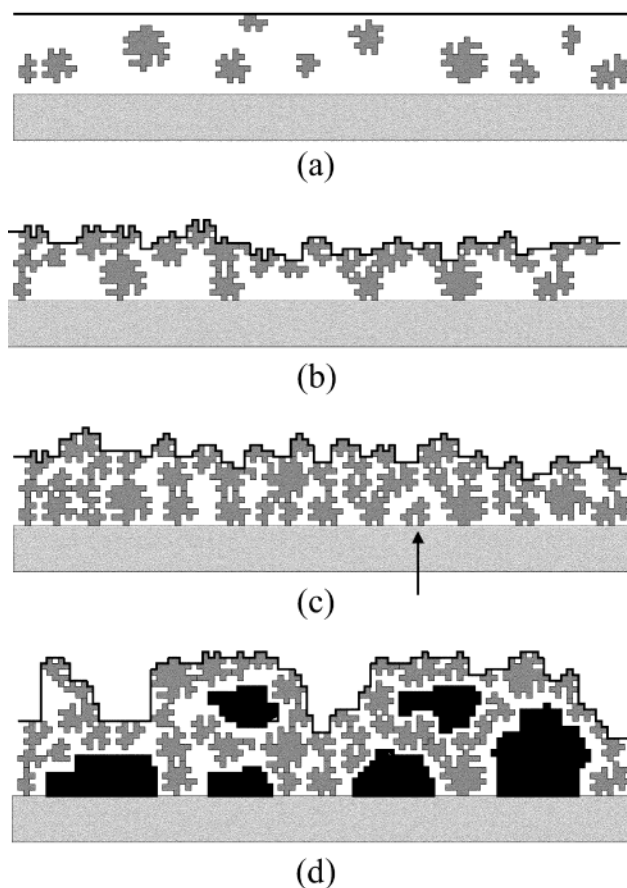


Figure 1. Schematic of the model of silica structure within dried lacquer. The low concentration regime (panel a, $m_{\text{sil}}/m_0 < 1$), the critical mass of silica (panel b, $m_{\text{sil}}/m_0 = 1$), and two possibilities for $m_{\text{sil}}/m_0 > 1$ are shown, with silica densification from collapse (panel c) or void formation with more robust silica (panel d). Note that (c) does not exclude the possibility of isolated silica particles, for example that marked in (c).

Table 1. Silica Bulk Densities, Specific Small Pore Volumes, and Critical Silica Mass Fractions

silica	ρ_{bulk} (g cm^{-3})	V_{pore}^* ($\text{cm}^3 \text{g}^{-1}$)	m_0 (mass fraction)
FS	0.0625	0.57	0.0219
FPS	0.0815	0.51	0.0285
UPS	0.138	0.47	0.0483
CPS	0.285	0.55	0.100

To find the critical silica concentration, the volume of lacquer must equal the volume of air between the silica particles, which can be determined as follows. The total volume occupied by the silica powder (silica and air) can be derived from the bulk density of silica (Table 1). Since the true density of bulk, pure silica is 2.18 g cm^{-3} ,⁸ the volume of silica is subtracted from the total to yield the volume of air.

However, the latex may not displace all the air. The silica is extremely porous and some pores may be too small for the latex spheres to penetrate. The volume of these small inaccessible pores is also subtracted from the bulk volume, yielding

$$V_{\text{dry}} = V_{\text{bulk}} - V_{\text{sil}} - V_{\text{pore}} \quad (2)$$

as the criterion for the critical silica mass fraction (Figure 1b). Here V_{dry} is the volume of dry lacquer, V_{bulk} is the bulk volume of dry silica powder, V_{sil} is the volume of silica (excluding air), and V_{pore} is the volume of small pores inaccessible to the latex.

(8) Iler, R. K. *The chemistry of silica*; John Wiley & Sons: New York, 1979.

(9) Kleinschmidt, P. *Spec. Publ.—R. Soc. Chem.* **1981**, *40*, 196–225.

(10) *Glascol C47, technical and processing data*; Coatings and Specialties Division, Allied Colloids Ltd.: Bradford, West Yorkshire, U.K.

(11) Granier, V.; Sartre, A. *Langmuir* **1995**, *11*, 2179–2186.

(12) Asbeck, W. K.; van Loo, M. *Ind. Eng. Chem.* **1949**, *41*, 1470–1475.

Table 2. Formulation Recipe

component	density (g cm ⁻³)	% by weight in formulation
80 nm polybutyl methacrylate latex binder	1.04	71.4
water	1.0	16.8
defoamer	1.0	0.1
silica matting agent	2.18	variable
coalescing aid	0.9	3.82
coalescing aid	0.922	1.91
defoamer	1.0	0.05
antiratering agent	1.04–1.07	0.5
surface enhancer	0.995	2.14
rheology modifier	1.07	0.8

Rearranging and substituting for mass yields⁴

$$m_0 = \frac{V_{\text{dry}}}{\left(\frac{1}{\rho_{\text{bulk}}} - \frac{1}{\rho_{\text{sil}}} - v_{\text{pore}}^*\right)} \quad (3)$$

where m_0 is the critical mass fraction of silica, ρ_{sil} and ρ_{bulk} are the true and bulk densities of silica, respectively, and v_{pore}^* is the volume of small pores in 1 g of silica, determined from porosimetry.¹³ A more complete derivation is given in refs 3 and 4.

3. Experimental Section

Sample Preparation. The different types of silica used are shown in Table 1. FS is fumed silica and the other three are all types of precipitated silica with different-sized aggregate particles; UPS is unsieved, while FPS is fine and CPS is coarse precipitated silica. The bulk density and values obtained for m_0 are given in Table 1 for these different silicas. The lacquer formulation is shown in Table 2. Ingredients are added in the order shown, at 1-min intervals and is the same for all the different types of silica. The silica was dispersed by use of a Cowles head rotating at 3000 rpm. Fifteen minutes of shear followed the addition of the last ingredient. The silica concentration was varied between $m_{\text{sil}}/m_0 = 0$ and $m_{\text{sil}}/m_0 \approx 2.8$. The specimens were left overnight prior to measurement. Further preparation details are given in ref 3.

Environmental SEM. By introducing a partial pressure of water vapor into the specimen chamber, ESEM effectively eliminates the charging effects of the incident electron beam that limit the use of conventional SEM with insulating specimens.⁶ This makes ESEM an ideal tool to examine the surface of matte lacquers.

Observed contrast in ESEM comes from two routes, backscattered and secondary electrons. Backscattered electrons are incident electrons, which have elastically scattered strongly in the specimen so that they are ejected and thus contribute to the signal. Incident electrons interact more strongly with the heavier atomic nuclei, so backscattered electrons are sensitive to atomic number.¹⁴ In this case, a bright signal is associated with the relatively high atomic number of silica with respect to the polymer film.

Secondary electrons are produced by ionization events in the sample and produce a strong signal at the detector. Secondary electrons have a rather small escape depth, on the order of a few nanometers. Since the penetration of incident beam electrons is much greater, the bulk of secondary electrons are produced deeper inside the specimen and reabsorbed. A sloping surface increases the chance of escape for secondary electrons at greater depths, so the signal is increased, giving rise to topographic contrast.¹⁴ Since surface roughness is related to the presence of silica at the surface,² a strong secondary electron signal from regions of surface silica is expected.

The ESEM used was an Electroscan E3 fitted with a LaB₆ thermionic source, with 12 keV beam voltage, 4 Torr chamber

pressure, and 7 mm working distance, which corresponds to a detector–sample distance of around 1 mm. The scan time was 17 s/frame, and the original magnification was 800 \times . The sample was electrically earthed, with silver dag between the chromated aluminum¹⁵ substrate and the ESEM stub. The films were prepared with a wet depth of 200 μm by use of a microapplicator.

ESEM Image Analysis. This image analysis technique has been detailed previously³ and is briefly recapped here. The technique seeks to isolate the pixels in the ESEM image which correspond to silica. Each pixel is therefore chosen as either silica or polymer, according to certain criteria. Although silica is bright in ESEM images, separating out which pixels belong to silica and which to polymer is not trivial. This is due primarily to small amounts of ESEM beam instability, which can significantly affect contrast and signal strength.³ However, silica is associated with a change in brightness, which is relatively insensitive to the absolute brightness of the signal. A gradient threshold is therefore used. This gradient threshold is based on the Sobel operator (S) operating on the image (Im):¹⁶

$$S(\text{Im}) = \sqrt{\left(\frac{\partial \text{Im}}{\partial x}\right)^2 + \left(\frac{\partial \text{Im}}{\partial y}\right)^2} \quad (4)$$

This Sobel operator tends to identify edges of silica particles, so the bright centers must be picked out by selecting pixels brighter than 245 on a scale from 0 to 255. A Sobel gradient threshold of 50 is used to identify the edges of the particles. If either or both criteria are satisfied, the pixel is identified as silica.⁴ A further criterion is to ignore isolated bright pixels, which in general are associated with noise.^{16,17} This is achieved by requiring that each group of bright pixels must contain more than 10 pixels to be treated as silica. The silica surface fraction is then found by dividing the number of silica pixels by the total in the image.⁴

Atomic Force Microscopy. The technique of tapping-mode AFM is well-known⁵ and only the briefest description will be given here. A constant separation between an extremely fine tip and a surface is maintained by ensuring a fixed interaction between the two. The height of the tip is then recorded as a function of lateral position to produce a surface map at nanometer resolution. In addition to this topographic contrast, AFM is also sensitive to the material properties of the specimen. The cantilever is oscillated at around 300 kHz in tapping mode to minimize the tip–specimen interactions, which is especially useful for delicate polymeric specimens. The lateral variation in viscoelastic response of the specimen gives rise to another source of contrast. This is referred to as phase contrast, on account of the change in phase of the oscillating cantilever tip introduced by the specimen response. Quantitative interpretation of phase contrast images is very hard indeed.¹⁸

For the samples studied here, the surface should be either film-formed latex or silica. There are other possibilities, such as surfactant exudation during film formation,¹⁹ but this should be a relatively small effect compared to the difference in viscoelastic properties between the silica in the polymer. Therefore, phase contrast should distinguish the relatively soft polymer from the harder silica.

A Digital Instruments Multimode AFM fitted with a Nanoscope 3 head and silicon nitride tip was used. Specimens were laid out on a 1 cm² piece of glass, by use of a razor blade in which was cut a shallow groove, 7 mm long and 0.2 mm deep. The groove was filled with lacquer and the razor blade was dragged across the glass, such that a layer of lacquer of nominal depth 200 μm was formed.

Reflection Measurements. The reduction in reflection introduced by the silica is determined by use of a white light

(15) Wernick, S.; Pinner, R. *Surface treatment of aluminum*, 4th ed.; Clare O'Moseley Ltd.: Moseley, Surrey, U.K., 1972.

(16) Russ, J. C. *The image processing handbook*, 2nd ed.; CRC Press: Boca Raton, FL, 1995.

(17) Pawley, J. B. *Handbook of biological confocal microscopy*, 2nd ed.; Plenum Press: New York, 1995.

(18) Bar, G.; Brandsch, R. *Langmuir* **1997**, *14*, 7343–7347.

(19) Tzitzinou, A.; Keddie, J. L.; Geurts, J. M.; Mulder, M.; Satguru, R.; Treacher, K. E. In *Film formation in coatings*; Proveder, T., Urban, M. W., Eds.; ACS Symposium Series; American Chemical Society: Washington, DC, 2001; Vol. 790, pp 58–87.

(13) G. Morea-Swift, personal communication, 2000.

(14) Goldstein, J. I. *Scanning electron microscopy and X-ray microanalysis*, 2nd ed.; Plenum Press: New York, 1992.

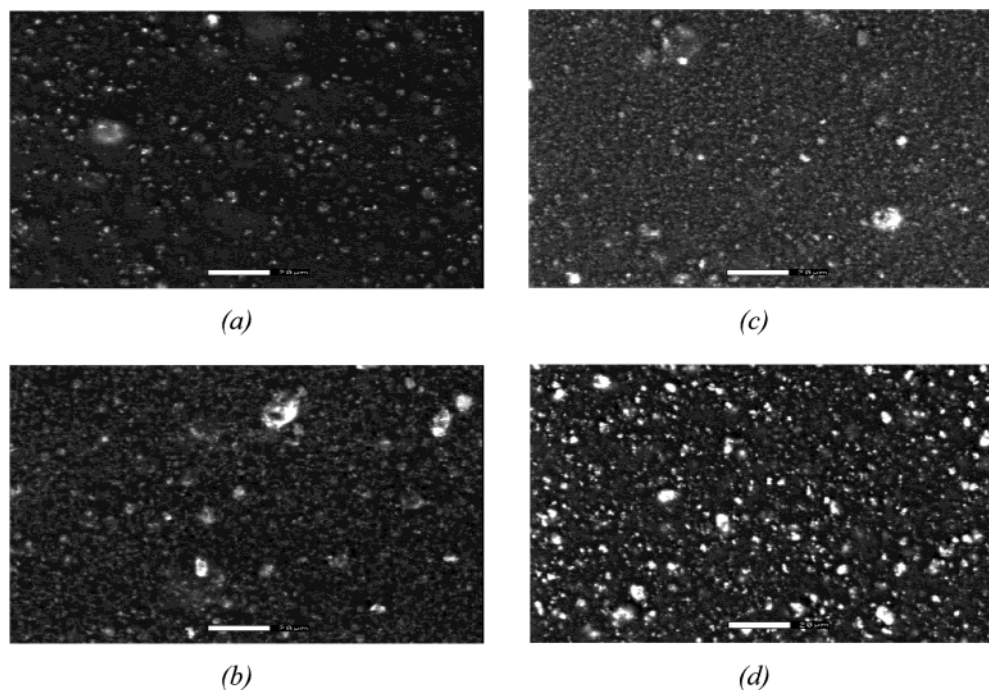


Figure 2. ESEM images of dried lacquer with fumed and fine precipitated silicas. Panels a–c show FS at $m_{\text{sil}}/m_0 = 0.47, 0.94,$ and 2.81 , respectively. Panel d shows FPS at $m_{\text{sil}}/m_0 = 0.93$. Bar = $20 \mu\text{m}$.

beam and measuring the intensity of the reflected beam on a Byk-Gardner gloss meter.⁴ Three angles between the incident beam and the normal (θ in eq 1) were used: $20^\circ, 60^\circ,$ and 85° . Here a lacquer without silica is taken as the reference. Although the lacquer is transparent, the major source of reflection is the air–lacquer interface, while the bulk of the lacquer film produces little reflected signal.⁴ However, the lacquer–substrate interface can contribute significantly to the reflected light beam.

These contributions from the lacquer–substrate interface were minimized with a nonreflecting substrate of sheet aluminum coated with an opaque matting coating. These “placquettes”¹³ were then sealed with a layer of lacquer without silica, which prevented the matte coating on the placquettes from introducing additional roughness on the film surface. The lacquer was laid down to a depth of $100 \mu\text{m}$ by use of a bar coater. The depth was $30\text{--}35 \mu\text{m}$ following film formation.

4. Results and Discussion

ESEM. ESEM images of dried lacquer containing FS are shown in Figure 2 for a range of silica concentrations, $m_{\text{sil}}/m_0 = 0.47, 0.94,$ and 2.81 in panels a–c, respectively. Silica is associated with bright regions, due to secondary and backscattered electron contrast, as discussed previously. There is a considerable increase in the amount of surface silica visible between panels a and b, with Figure 2a seeming to correspond to the condition of Figure 1a, and 2b to 1b. However, there appears to be very little difference at all between Figure 2 panels b and c. It would seem that the weakly bound fumed silica forms a structure, which collapses at high m_{sil}/m_0 , leading to little change of surface silica content at high silica concentrations. Thus the high silica concentration behavior appears to match that of Figure 1c. Collapsing of fumed silica has also been demonstrated in a separate experiment on the bulk of the lacquer film.⁴

Figure 2d shows fine precipitated silica (FPS) at $m_{\text{sil}}/m_0 = 0.93$, with a generally similar appearance to the fumed silica. Interestingly, the contrast is rather better than for the FS and the surface does appear somewhat different. The FS surface morphology is relatively homogeneous throughout the image (Figure 2b), whereas the FPS particles are somewhat more distinct.

The unsieved precipitated silica (UPS) (Figure 3a–c) shows a similar appearance to the FPS, although there are some larger particles present. Most interestingly, the UPS has a considerable increase in surface silica content at high silica concentration (Figure 3c), unlike the FS (Figure 2c). This suggests a structure similar to that of Figure 1d where the silica resists collapse, which implies that the precipitated silica structure is at least more robust than the fumed silica. This is in keeping with the ultimate particles being covalently bound to form aggregates in the precipitated silica, as opposed to the hydrogen-bonded fumed silica.

The coarse precipitated silica is shown in Figure 3d, $m_{\text{sil}}/m_0 = 0.72$, has some very large particles, up to $10 \mu\text{m}$ in size. This is expected from the sieving; the smaller particles are presumably the result of fragmentation during storage and mixing.

By the ESEM image analysis technique, the fraction of pixels corresponding to silica (i.e., the silica surface fraction) is plotted in Figure 4a for fumed silica and b for the different precipitated silicas. Each point is typically the mean of six images with the error bars marked being the standard error. The difference between the fumed and the precipitated silicas is clear. Silica surface fraction does not increase beyond $m_{\text{sil}}/m_0 \approx 1.5$ for FS, as anticipated from simple visual inspection of the images, but up to this silica loading, there is a quasi-linear increase in surface silica fraction as a function of m_{sil}/m_0 . Straight-line regression fits have been applied to both regimes, as shown in the figure. Both the intercept in the $m_{\text{sil}}/m_0 < 1.5$ region and the slope of the $m_{\text{sil}}/m_0 > 1.5$ regime are equal to 0 within error bounds.

By contrast, for the precipitated silica, surface silica fraction increases at all silica concentrations (Figure 4b). In fact, the data for all precipitated silicas appear to fall broadly on the same line. This is plotted as silica surface fraction = $1 - \exp(-m_{\text{sil}}/m_0)$. This functional form is required because the surface silica fraction must not exceed unity but has no obvious further physical meaning.

It is interesting that all the PS points fall on the same

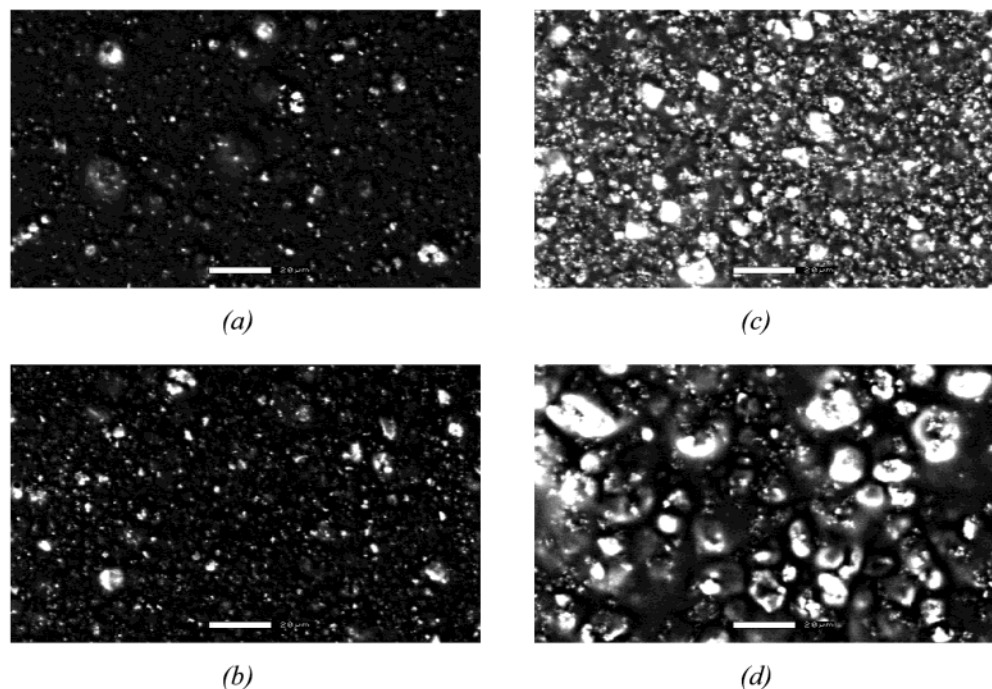


Figure 3. ESEM images of dried lacquer with unsieved precipitated silica (panels a–c, $m_{\text{sil}}/m_0 = 0.43, 0.87,$ and $2.18,$ respectively) and coarse precipitated silica (panel d, $m_{\text{sil}}/m_0 = 0.72,$ showing large particles). Bar = $20 \mu\text{m}$.

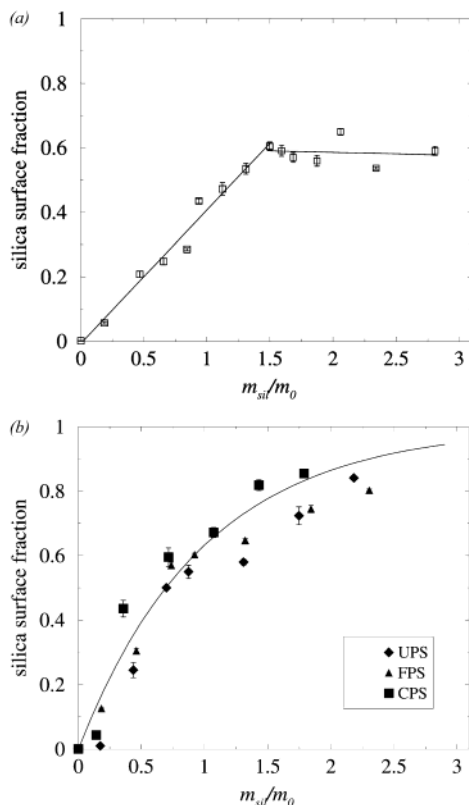


Figure 4. Silica surface fraction as a function of m_{sil}/m_0 : (a) fumed silica and (b) precipitated silicas. The surface silica fraction ceases to rise beyond $m_{\text{sil}}/m_0 \approx 1.5$ in the FS case, whereas for all precipitated silicas it increases to approach unity.

line, for silicas of widely differing bulk densities (Table 1). This clearly shows that the silica surface is dominated by the bulk *volume* rather than the mass of silica added to the formulation. Figure 4b provides strong evidence for a surface structure dependent on silica bulk volume, as assumed in the model.

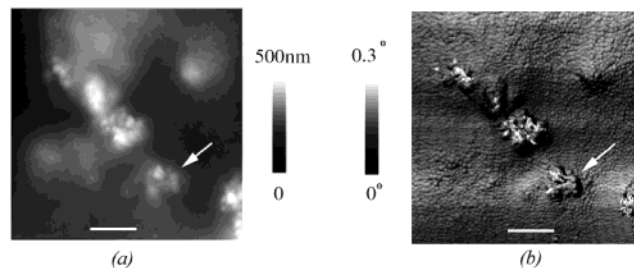


Figure 5. AFM images showing silica and latex particles for UPS at $m_{\text{sil}}/m_0 = 1.8$. Higher regions in the topographic image (a) reveal peaks associated with silica particles, whereas phase contrast (b) shows partially deformed latex particles. Bars = $1 \mu\text{m}$.

Atomic Force Microscopy. Due to its very high resolution, AFM reveals structure on a smaller length scale than that accessible to ESEM. Raised regions are taken to be silica (such as that marked with an arrow in Figure 5a). More interestingly the phase contrast image (Figure 5b) reveals circular regions around 80 nm across, which are interpreted as partially deformed latex spheres. The latex has been shown to be 80 nm in diameter in a separate light scattering experiment. The fact that these spheres have not deformed completely after 24 h is not surprising: full deformation can take weeks.²⁰

From the AFM images, it appears that the surface is actually predominantly composed of deformed latex spheres, rather than silica particles (which would be larger and irregular). Hence this implies that the silica particles are covered in the partially deformed latex (arrows in Figure 5). At first sight this conclusion is somewhat surprising, given the appearance of the ESEM images, with up to 80% of the surface identified as silica. To reconcile the AFM and ESEM images, it is necessary to reconsider what the images in Figures 2 and 3 are actually showing. ESEM is sensitive to both surface roughness

(20) Lin, F.; Meier, D. J. *Langmuir* **1995**, *11*, 2726–2733.

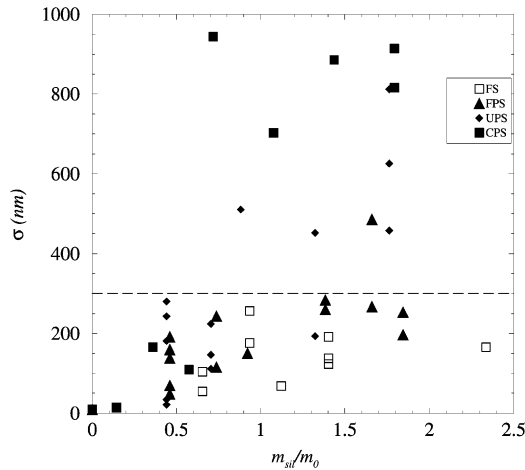


Figure 6. Surface standard deviation σ as a function of m_{sil}/m_0 . The coarse and unsieved precipitated silicas with larger more robust particles have a far greater surface roughness (for m_{sil}/m_0 greater than 1) than the other silicas. FS and FPS data points fall below $\sigma \approx 300$ nm (black dotted line).

(via secondary electrons) and silica (via backscattered electrons). Backscattered electrons emitted from the surface are produced at depths up to several micrometers into the specimen at the beam energy used¹⁴ and so can reflect subsurface silica particles. Secondary electrons reflect the surface topography, rather than silica as such.¹⁴ Pulling these ideas together means that the ESEM images can be interpreted as a roughened surface with subsurface silica, in agreement with the AFM results.

To make quantitative measurements of surface roughness, an area larger than the length scale of the silica particles must be scanned. Since the silica particles are up to 10 μm in size, and the AFM is limited to 100- μm scans, 30- and 60- μm scans were used to determine surface roughness. No differences were seen between these two scan sizes, so the data are presented together. The standard deviation of the local height from the mean, σ , is given by

$$\sigma = \sqrt{\frac{1}{N-1} \sum_i (h_i - \bar{h})^2} \quad (5)$$

with N the number of pixels in the image, h_i the height of each pixel, and \bar{h} the mean height.

The results for the surface standard deviation, σ , are plotted in Figure 6 as a function of m_{sil}/m_0 . Although the number of data points is rather small (due to the relatively slow rate of image acquisition in AFM and lack of instrument time), we can draw some conclusions from Figure 6. The standard deviations above $m_{\text{sil}}/m_0 \approx 0.7$ appear to be grouped according to particle size. The larger coarse precipitated silica particles have a large $\sigma > 700$ nm, whereas the unsieved precipitated silica particles have a σ lying in the range $300 \text{ nm} < \sigma < 700$ nm. The silicas with smaller aggregate particles, FS and FPS, have $\sigma < 300$ nm for all m_{sil}/m_0 . From these data it is clear that the surface standard deviation is strongly influenced by the average silica particle size.

However, this is not the only determining factor; silica volume fraction is important as well. At low m_{sil}/m_0 , σ is less than 300 nm for all silicas. Thus as long as there is not much silica in the sample, little surface roughness develops, even if the particles are quite large. The exception to this is the case for $m_{\text{sil}}/m_0 = 0.72$ for CPS. In this case, although still below the critical silica volume

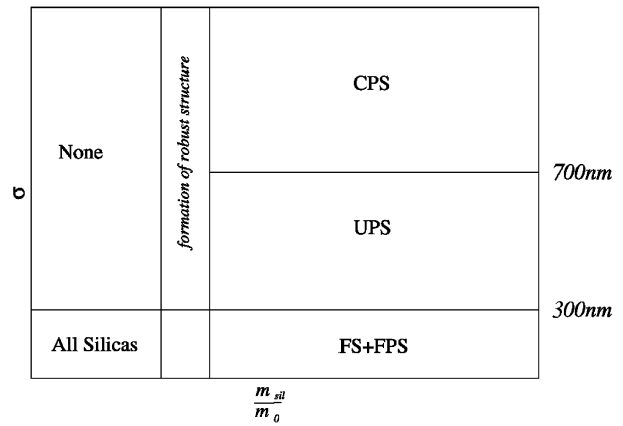


Figure 7. Schematic of Figure 6, summarizing surface height standard deviation behavior for different silicas. The range of σ of each type of silica is shown, for different m_{sil}/m_0 regimes.

fraction, it is not unreasonable to suppose that as m_{sil}/m_0 tends to unity, the silica structure resists collapse enough to affect the surface, as the structure tends toward that in Figure 1d. After all, at low silica concentration, σ is much reduced. This dramatic difference suggests that surface roughness is determined by a silica structure of many small particles, rather than individual large particles (although, for the CPS in particular, single particles could conceivably also contribute). The increase in surface roughness around the critical silica concentration of $m_{\text{sil}}/m_0 = 1$ is consistent with the assumption of many silica particles supporting each other, as shown in Figure 1b. If the surface roughness were dependent purely on individual large silica particles, then it would increase gradually with silica concentration, without the sudden increase around the critical silica concentration that we see for both CPS and UPS.

In contrast to this behavior, there is no change in σ around the critical silica concentration for FS and FPS. Now the analysis of the ESEM results above indicates a distinction between fumed and precipitated silicas. Fumed silica collapses completely, but precipitated silica undergoes at most only partial collapse. This apparent discrepancy between ESEM (FPS behaves as UPS and CPS) and AFM (FPS behaves as FS) is reconciled as follows: The inclusion of any silica at all increases the standard deviation from around 10 nm (no silica) to between 100 and 300 nm, as can be seen in Figure 7. Any structuring of the silica would need to produce a standard deviation significantly more than 300 nm to indicate its presence. That no change in surface roughness occurs as the critical silica concentration is passed therefore indicates that the structures formed by both FS and FPS aggregates are too small to make a difference to the surface roughness, whether a robust structure is formed or not. Surface roughness is summarized in Figure 7, a schematic of Figure 6. Different silicas populate the various regions of this σ vs m_{sil}/m_0 diagram.

Reflection. Reflection measurements were carried out for three incident angles, with the same white light source. Those for an angle to the incident of 85° are presented. According to the theory of Gate et al.,⁷ a relationship should exist between reflectance and the surface roughness σ . In the earlier work,⁷ such an analysis was used to extract σ , but for the samples used here the value of σ has been directly and independently obtained, from AFM measurements, so a better test can be made. The previous section has shown that σ depends on a variety of parameters including silica type (and hence particle size) and tendency

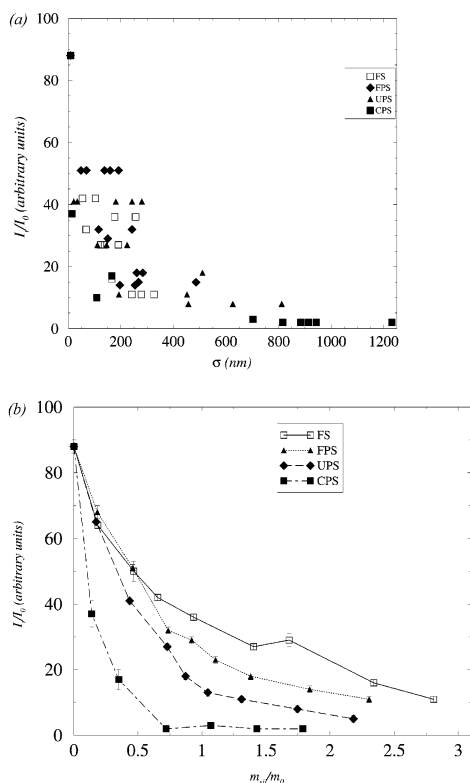


Figure 8. Reflection as a function of surface height standard deviation obtained from AFM (a) and m_{sil}/m_0 (b). Panel a shows a continuous decrease in reflection for increasing surface roughness. In panel b we see the change in reflection behavior between the different silicas for the same volume fraction of silica added to the formulation.

for collapse of silica structure and the ratio m_{sil}/m_0 (Figure 6), and so we might expect the reflection measurements to depend on these parameters too.

Figure 8a shows how the reflectance depends on σ . There is a significant amount of scatter in this plot, although there is a clear trend of decreasing reflection with increasing surface roughness, as expected. The fall of reflectance extends to a value of σ of ~ 300 nm, after which the decrease is much smaller. As was shown in Figure 6, all the data points for FS and FPS fall within this range, whereas the silicas with larger and more robust particles give rise to greater surface roughness. If reflectance is plotted as a function of m_{sil}/m_0 (Figure 8b), then each silica falls on a distinctly different curve. The CPS shows the fastest falloff, consistent with the roughest surfaces being generated. The falloff flattens off beyond a value of m_{sil}/m_0 of around 0.7. The value of m_{sil}/m_0 at which the curves in Figure 8b flatten off increases as the average particle size decreases.

The theory of Gate et al.⁷ can be directly compared with the data here. Figure 9 shows a plot of $\ln(I/I_0)$ as function of σ^2 for values of σ up to around 300 nm and an angle to the normal of 85° . This upper limit has been set since, for values of σ above 300 nm, the relationship in eq 1 is found not to be linear. For these larger values of σ , the horizontal length scale of the surface roughness begins to exceed the wavelength of light (Figure 3d), so a different type of behavior is not unreasonable. The data clusters round a line of best fit with whose gradient is given in eq 1. All the parameters are known except the wavelength of the incident light, λ . Solving eq 1 for λ gives a value of 509 nm for the results plotted in Figure 9, which is reasonable for a white light source. However, at smaller angles to the normal, the theory predicts a faster falloff of $\ln(I/I_0)$ with

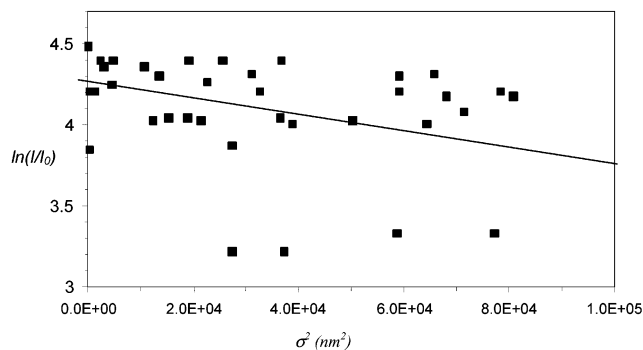


Figure 9. Plotting the logarithm of the reflection as a function of the variance of the surface produces results consistent with the straight-line behavior expected from eq 1.

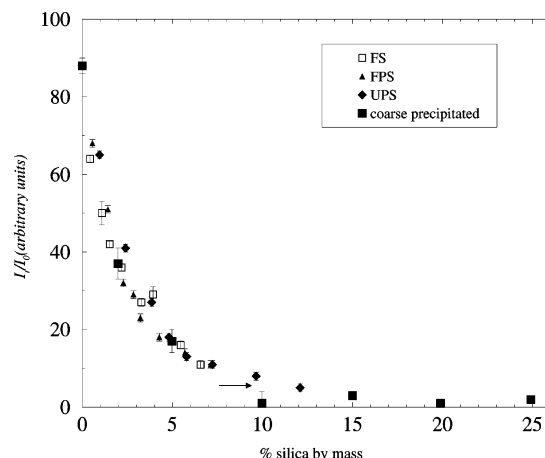


Figure 10. Spectral reflectance appears to be a function of silica mass fraction rather than volume fraction (Figure 8b).

increasing σ than that which we measure. We believe this may be associated with subsurface scattering. Closer to the normal, more light is scattered nonspecularly, which would result in less reflection on relatively smooth surfaces than the Gate theory⁷ allows for, as it does not consider the bulk of the film.

What is surprising is that if the data of reflectance are now plotted against the percentage silica mass, all the different samples appear to fall on a universal curve. Although this behavior looks very striking, it is thought to be more coincidence than relating to underlying physics (Figure 10). The silicas have very different densities and their contribution to surface roughness is not simply dependent on volume fraction (Figure 8b). However, although the silicas have widely varying bulk densities and particle sizes, there is a strong correlation between aggregate particle size and bulk density (Figures 2 and 3, Table 1). Smaller aggregate particles (FS, FPS) producing low roughness (and hence high reflection) have low bulk density, so only a relatively low mass fraction is added, for all silica volume fractions. Conversely, denser silicas (UPS, CPS) have large particles producing more surface roughness, so for the same volume fraction, more mass of silica is added and the larger aggregate particles disrupt the surface more, reducing reflection. It turns out that reflection appears to follow silica mass fraction, rather than bulk volume fraction, due to the differing bulk densities of the large and small aggregate silica particles (Figure 10a).

5. Conclusions

The surface microstructure of the matte water-based lacquer has been determined with ESEM and AFM. This

microstructure along with measurements of optical reflection has been linked to the work of Gate et al.⁷ The experimental results have been shown to support the model of silica structure in the lacquer.

There is relatively little silica present on the surface of the film. It has been shown by AFM to be covered in a layer of partially deformed latex. Fumed silica undergoes structural collapse above the critical silica mass fraction. The silica structure is assumed to be crushed under the compressive forces introduced by water evaporation during film formation, which is in agreement with related studies of the bulk of these same lacquers.⁴ This collapse means that the standard deviation of the surface of fumed silica is limited to around 300 nm. Precipitated silica also appears to collapse, as the smaller FPS fraction exhibits similar surface roughness behavior to that of the fumed silica. However, precipitated silica resists collapse at least to some extent, as more silica is found in the surface region at high silica concentrations. Furthermore, larger precipitated silica particles produce a very considerable increase in surface roughness around the critical silica volume fraction.

The results presented in this article are consistent with a linear relationship between the variance of the surface

height and the logarithm of the reflected intensity. This trend is in agreement with earlier work carried out by Gate et al.⁷ Where the angle to the normal is large (85°) and there is little subsurface scattering, there is quantitative agreement with the theory. We find that, at smaller angles to the normal (20° and 60°), the agreement is qualitative only.

Now that the surface roughness parameter σ is linked to the silica particle size and is also inversely related to reflection, reflection also appears to be a function of silica mass fraction. However, the AFM work leads us to suppose that surface roughness is truly a function of bulk silica volume as predicted by the model, with the mass dependence a result of increasing bulk density of large aggregate particles, which cause more surface roughness due to their size.

Acknowledgment. We thank Dr. K. Dalnoki-Veress, Dr. J. Forrest, and Professor R. Jones at Sheffield for their help with the AFM, and the EPSRC and Crossfields for a CASE award to C.P.R.

LA025776N